Low frequency electrochemical noise in AlGaN/GaN field effect transistor biosensors

Paul Bertani, Yuji Wang, Hao Xue, Yi Wei, and Wu Lu

View Online   Export Citation   CrossMark

ARTICLES YOU MAY BE INTERESTED IN

AIP Publishing

Low frequency electrochemical noise in AlGaN/GaN field effect transistor biosensors

View Online   Export Citation   CrossMark

Paul Bertani, Yuji Wang, Hao Xue, Yi Wei, and Wu Lu[a] (iD)

AFFILIATIONS

Department of Electrical and Computer Engineering, The Ohio State University, Columbus, Ohio 43210, USA

[a]Author to whom correspondence should be addressed: Lu.173@osu.edu

ABSTRACT

Little has been studied on how the electrochemical noise impacts the limit of detection of field effect transistor (FET) biosensors. Herein, we investigate low frequency noise associated with phosphate-buffered saline (PBS) solutions at varying ionic strengths (N_i) under both weak and strong gate biases corresponding to saturation and sub-threshold regimes, respectively, in AlGaN/GaN heterojunction FET biosensors. We show that the electrochemical noise is strongly dependent on the ionic strength and gate biasing conditions. In the saturation regime (low bias), varying the ionic strength (a range of $10^{-6} \times$ PBS to PBS $1 \times$ stock solutions used for testing) has little to no effect on the characteristic frequency exponent $\beta(\beta = 1)$, indicating a predominately diffusion-based process. Conversely, under higher biases (sub-threshold regime), the β parameter varies from 1 to 2 with ionic strength exhibiting both diffusion and drift characteristics, with a "cut point" at approximately $10^{-5} \times$ PBS ($N_i \approx 9 \times 10^{14}$/mL). Under a high bias, once the PBS concentration reaches $10^{-3} \times$, the behavior is then drift dominant. This indicates that the higher bias likely triggers electrochemical reactions and by extension, faradaic effects at most physiologically relevant ionic strengths. The signal-to-noise ratio (SNR) of the device has an inverse linear relationship with the low frequency current noise. The device exhibits a higher SNR in the sub-threshold regime than in the saturation regime. Specifically, within the saturation regime, an inversely proportional relationship between the SNR and the ionic concentration is observed. The electrochemical noise induced from ionic activities is roughly proportional to $N_i^{-1/2}$.

Modern biosensors are commonly reported, showing the detection of a wide variety of analytes on many different material platforms.[1–13] Among these, AlGaN/GaN HEMTs (High Electron Mobility Transistors) offer an attractive platform for constructing a biosensor. AlGaN/GaN heterostructures offer good biocompatibility with cells and biological elements, wide bandgap, good stability in a wide range of thermal conditions and chemical environments, and a highly sensitive channel.[14–16] Such devices have demonstrated the ability to detect an abundance of analytes at low concentrations such as DNA and proteins.[17,18] Biosensors are typically described by several criteria including sensitivity, selectivity, cost, and easiness of operation. Of these, sensitivity is often a critical figure of merit that determines if a biosensor can be used for a given application.

In order to develop biosensors with high sensitivity, a critical criterion must be addressed—the deleterious influence of noise on the device signal. The noise intrinsic to the system is a key factor in determining the "low end" of a device's dynamic range curve or the window of operation in which the device functions properly. This is also sometimes referred to as the LOD (limit of detection) or MDL

(minimum detectable limit).[19] Noise that is unavoidable or intrinsic to the system can come in many forms, such as (1) thermal noise due to ionic motion, (2) intrinsic noise from the device itself, (3) noise due to the ionic motion of biomolecules in solution or at the active region interface, and (4) noise due to electrochemical reactions or faradaic processes at the electrode-electrolyte interface.[20–22] This noise can manifest itself as the often discussed 1/f or low-frequency noise. Low-frequency noise is of primary concern in biosensor devices as they typically operate under DC biasing conditions, and additionally, the binding and unbinding of analytes to a receptor is a low-frequency event. However, the effects of these phenomena related to the overall device sensitivity in various setups have not been well studied. By examining the low frequency noise characteristics of a specific device platform, one can get an idea of the hypothetical maximum sensitivity that the platform can achieve and under what conditions noise considerations will have a significant impact.

The AlGaN/GaN HEMT serves as an ideal platform for noise-related studies due to its innate chemical stability under variable conditions. A cross-sectional illustration of the AlGaN/GaN HEMT used
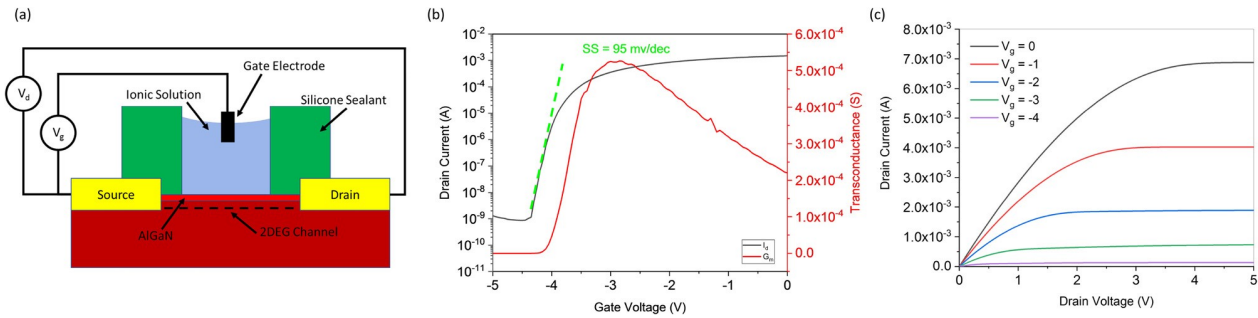
FIG. 1. Device structure and DC characteristics of AlGaN/GaN HEMTS in DI water: (a) cross-sectional illustration of the AlGaN/GaN HEMT biosensor system showing the 2DEG channel connecting the two metal contacts, silicone reservoir sealing, and liquid gate. (b) Transfer characteristics demonstrating a peak I_d at 1.5 mA under a 0.5 V bias (V_d) and a threshold of approximately -4 V. The sub-threshold slope is denoted by "SS" and is approximately 95 mV/decade. The transconductance (gm) is shown on the right axis in red. (c) Family I–V sweeping from 0–5 V with gate voltages from $V_g = 0$ V to $V_g = -4$ V in 1 V increments.

in this study is shown in Fig. 1(a). This illustration shows the layout of the device itself for visualization on how biases are applied and determine potential sources of noise, which are unavoidable in such a setup. Devices were fabricated using an AlGaN/GaN wafer with a 23 nm AlGaN barrier layer and 2 μm GaN on the SiC substrate. Mesa isolation was done via dry etching using BCl_3/Cl_2 plasma. Following mesa isolation, a Ti/Al/Mo/Au metal stack was put down via a CHA metal evaporator and annealed after lift-off for Ohmic contacts at 850 °C for 30 s. An overlay layer of Ti/Au was used for source/drain probing robustness. Silicone was used to form a micro-reservoir for PBS (phosphate buffered saline) solution and gating through a reference electrode as the gate. The gate has a width of 2 mm and a length of 1 mm.

DC measurements were performed using a probe station and an Agilent 4156C Semiconductor Parameter Analyzer. Using a micropipette, approximately 15 μl of solution was added to the gate/active region for each test. The device surface was cleaned via a rinse with DI (de-ionized) water after each trial. PBS solutions were prepared with varying strengths, from $10^{-6} \times$ PBS to PBS 1 × (stock) strength ionic strength ranges corresponding to (1.627×10^{-8} M–162.7 mM, respectively). All PBS solutions were diluted from Thermo Fischer Scientific 1 × PBS stock. The DC characteristic curves (transfer characteristics and family I–Vs) for the AlGaN/GaN HEMT in DI water for this study are shown in Figs. 1(b) and 1(c). The measured key device parameters include I_{dss} (drain current at $V_g = 0$ V) = 6.88 mA at $V_d = 5$ V, the off-state current $I_{off} = 0.86$ nA, the current on/off ratio = 2×10^6, the sub-threshold slope $SS = dV_g/ dlog(I_d)$ (where I_d is drain current) is 95 mV/decade, the maximum transconductance $G_{m\_MAX} = 0.53$ mS, and the threshold voltage $V_{th} = -4$ V.

Noise measurements were performed using an Agilent 4440A Spectrum Analyzer in conjunction with a SR570 lock-in amplifier. SR 570 is used to both bias the drain terminal at 0.5 V and account for the device current offsets, where $I_d = 200$ nA and 1 mA in the sub-threshold and saturation regime cases, respectively. The biasing strength on the gate electrode, the presence of salts and biomolecules, and intrinsic device noise would have significant impacts on the low-frequency noise of the system. Notably, real measurements are most often performed in a buffer solution, serum, or other high salt environments, and thus, high gate biases may trigger electrochemical reactions

in the liquid gate or "active region" and easily facilitate redox processes if the proper conditions are met. When evaluating biasing considerations using an FET-based biosensor platform, one fundamental question to answer is what the optimum biasing condition is. For the maximum signal readout, the device is biased at the voltage that gives the maximum transconductance (g_m).[23,24] At this condition, the current change (ΔI_d)

$$\Delta I_d = \Delta V_g g_m, \qquad (1)$$

where ΔV_g is the gate surface potential change due to the specific binding between receptors immobilized on the sensing area and analytes in the solution. The signal-to-noise ratio (SNR) under this condition,

$$SNR = \frac{|\Delta I_d|}{\delta_i} = \frac{\left| \int_{V_{g1}}^{V_{g2}} g_m dV_g \right|}{\delta_i} \approx \frac{\Delta |V_g| g_m}{\delta_i} = \frac{|\Delta V_g| g_m}{\sqrt{S_i}}, \qquad (2)$$

where δ_i is the current noise, V_{g1} and V_{g2} are the gate potential before and after analyte binding events, and S_i is the current noise power ($S_i = \delta_{i^2}$).

Another way to look at the device is under what bias condition the device would give the maximum relative current change to the base current. In this case, the device should be biased at the subthreshold due to the exponential relationship between the gate bias and channel current.[25–27] In the sub-threshold regime, the drain current can be expressed as follows:

$$I_{d_{sub_{th}}} = I_{th} \exp\left[\frac{q(V_g - V_{th})}{mkT}\right], \qquad (3)$$

where I_{th} is the threshold current, k is the Boltzmann constant, T is the temperature in Kelvin, q is the electron charge, and m is the factor governing the subthreshold slope with a value of 1.59 [$SS = kTln(10)(1+m)$] as shown in Fig. 1(b). Therefore, the relative current change due to sensing with potential change ΔV_g is

$$\frac{|\Delta I_d|}{I_d} = \exp\left[\frac{q|V_g|}{mkT}\right] - 1. \qquad (4)$$

Under this condition and consideration, we have

$$SNR = \frac{\frac{|\Delta I_d|}{I_d}}{\frac{\sqrt{S_i}}{I_d}} = \frac{\exp\left[\frac{q|V_g|}{mkT}\right] - 1}{\delta_{in}}, \quad (5)$$

where δ_{in} is the normalized current noise ($\delta_{in} = \frac{\delta_i}{I_d} = \sqrt{S_i}/I_d$).

Finally, a device may be operated in the saturation regime for maximum drain current. Depending on which bias regime is selected, the device, and by extension the gate electrode, may be subject to very different voltage levels, from strong to relatively weak. To investigate this phenomenon, in this work, two gate biasing conditions were chosen. One biasing condition of -4.2 V is selected for the "high bias" scenario, and the device is operated in the sub-threshold regime under this bias. For the "weak bias" condition, -1 V is selected to bias the device in the saturation regime while keeping the bias below the water disassociation potential (1.23 V). The measured noise spectra in the saturation regime are shown in Fig. 2(a) as a function of frequency from 3–1000 Hz for PBS strengths of $10^{-5} \times$ to $1\times$. In all PBS solutions, the device exhibited similar $1/f$ noise characteristic behavior with respect to the slope. This curve is then fitted via a power fit to determine the characteristic slope value in each case using Hooge's empirical equation below:[28]

$$S_i(f) = \frac{\alpha_H I^2}{f^\beta N}. \quad (6)$$

Here, the noise power is related to the Hooge constant (α_H), the carrier number (N), signal (drain) current, frequency (f), and the characteristic frequency exponent (β). Using the fitted curves and Eq. (2), the SNR values for the saturation regime can be determined. Assuming a small gate potential change where the transconductance is treated as a constant, for PBS $10^{-5}\times$ through $1\times$, the SNR per volt values are found to range from 7.65×10^4 to 8.53×10^5 V^{-1} at f = 5 Hz. The extracted β values for the saturation regime at each investigated PBS strength are shown in Fig. 2(b). Notably, β remains essentially constant throughout the concentration range at a value close to 1. We note that, however, higher ionic strengths appear to be correlated with lower noise power. It is believed that this is due to the electrical screening effect. Specifically, the charge noise is the result of ionic perturbations within a few Debye lengths and a higher ionic strength leads to a smaller Debye length. To confirm this, we plot the current noise power as a function of Debye length (λ_d) in Fig. 2(c). Indeed, a linear relationship is observed on a log–log plot and a positive correlation is confirmed. This also reinforces that the total noise is significantly influenced by ionic processes. Here, the Debye length

$$\lambda_D = \sqrt{\frac{\varepsilon_0 \varepsilon_r kT}{2N_A q^2 N_i}}, \quad (7)$$

where ε_0 is the permittivity of free space, ε_r is the dielectric constant of electrolyte, N_A is Avogadro's number, and N_i is the ionic concentration in molar. More specifically, we observed a relationship between noise power and ionic strength of the form $S_i = S_{int} + \gamma N_i^{-1/2}$. These two components correspond to the intrinsic device noise (S_{int}) at given biases and the electrochemical noise power influence from the ionic liquid, which is inversely proportional to $N_i^{-1/2}$ with a factor of γ.

After examining the low bias/saturation scenario, the high bias or sub-threshold regime is investigated, with the results shown in Fig. 3(a). Compared to the saturation regime case, which has a relatively uniform slope throughout the measured frequency range, the sub-threshold regime measurements consistently show a corner frequency separating two frequency regimes: one regime at lower frequencies (approximately 3–50 Hz) with a higher slope (denoted as region 1) and the other regime with a lower slope at higher frequencies (50–60 Hz onward, denoted region 2) that gradually transitions to the noise floor. $1/f$ and $1/f^2$ lines are shown in Fig. 3(a) for ease of comparison. The first observation is that as the ionic strength increases, the characteristic frequency slope β varies from 1 to 2. In a real analyte binding scenario, within the sub-threshold regime, if the gate potential shift due to analyte binding is very small ($\Delta V_g < 5$ mV), then the SNR is close to a linear function of ΔV_g. In this case, the device exhibits SNR per volt values of 2.46×10^6–3.79×10^7 V^{-1}. If ΔV_g is sufficiently large ($\Delta V_g > 3$ mkT/q, ≈ 125 mV for this device), then the SNR is an exponential function of ΔV_g. For example, the SNR ranges from 1.96×10^6 to 3.05×10^7 at $\Delta V_g = 125$ mV (f = 5 Hz) for our devices using Eq. (5).

The extracted β values in the sub-threshold regime for each PBS concentration are shown in Fig. 3(b). β begins around approximately 1 at low ionic strengths, but then gradually increases as the PBS
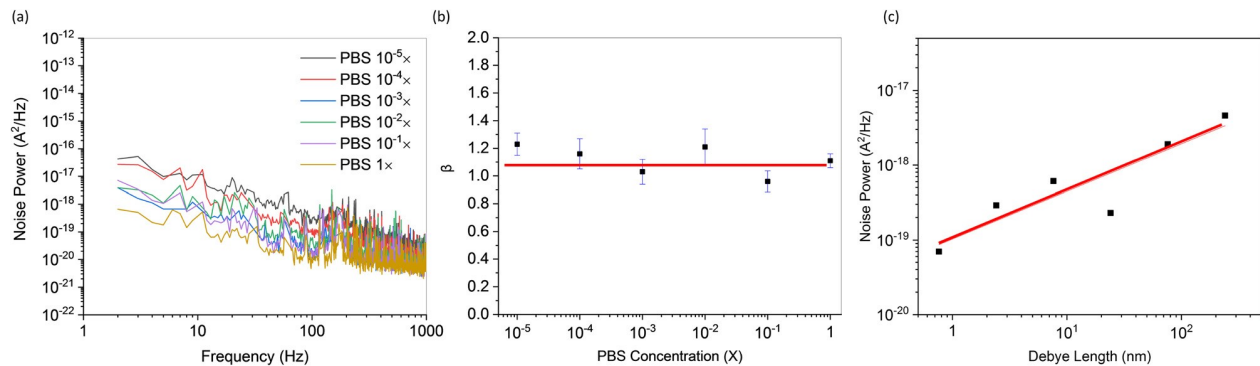
FIG. 2. Saturation regime ($V_g = -1$ V; $V_d = 0.5$ V) low frequency noise results. (a) Measured current noise power (S_i) with PBS solution ionic strengths ranging from $10^{-5} \times$ to $1 \times$ PBS. (b) The fitted frequency exponent value (β) shows a near constant value slightly above the expected result of $\beta = 1$ (red line shown for reference). (c) Log–log scale plot of noise power (S_i) vs Debye length (λ_D) for a full range of PBS concentrations with a linear fitting displayed via a red line.
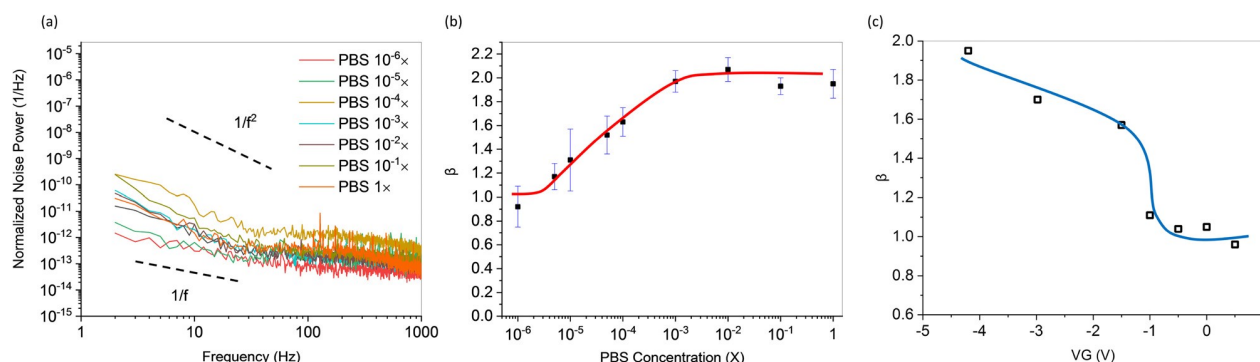
FIG. 3. Low frequency noise results in the sub-threshold regime ($V_g = -4.2$ V; $V_d = 0.5$ V) and noise frequency exponent (β) values vs gate voltage. (a) Measured normalized (by current) noise power ($S_i/I_d^2 = \delta_{in}^2$) with the range of PBS solution ionic strengths from $10^{-6} \times$ to $1\times$ PBS, all showing two frequency regimes. β values are only considered in the lower frequency region. 1/f and 1/f^2 dashed lines are shown for reference. (b) PBS concentrations vs frequency exponent β values in the subthreshold regime ($V_g = -4.2$ V), showing a flat region ($\beta = 1$), then moving to a transition region between PBS concentrations $10^{-5} \times$ and $10^{-3} \times$, and then saturating when $\beta \approx 2$. (c) β as a function of gate voltage ($V_g = -4.2$ V-0.5 V; $V_d = 0.5$ V), where from 0.5 V to -1 V, β is nearly constant and then undergoes a rapid increase as the device is biased toward threshold due to electrochemical phenomena.

concentration, and thus the ionic strength, is gradually increased. A "cut point" is apparent at a strength of roughly $10^{-5} \times$ PBS. Following this point, the β value consistently increases until it reaches a value of approximately 2 and remains constant with a PBS strength of $10^{-3} \times$ or greater. In general, when investigating low-frequency noise effects in electrochemical sensors and how they impact device noise, two electrode interface models have been proposed: non-faradaic or IPE (ideal polarized electrodes) and faradaic type electrodes.[29] When considering an IPE, it is modeled as an ideal capacitor that is not subject to the influence of redox reactions at the interface. The charge transfer in this IPE process is considered dominated by a diffusion process. In contrast, a faradaic electrode causes redox reactions and processes that might occur at the gate electrode-aqueous media interface under certain conditions, specifically when the device is under a significantly strong voltage bias. In this case, the charge transfer process is considered dominant by a drift process. Depending on the electrochemical processes at the electrode-electrolyte interface, the low frequency noise has different β values[30] corresponding to one of these two scenarios (or a combination of both). In the IPE or non-polarized case (i.e., slow or negligible redox processes), only diffusion movement occurs, which has a 1/f relationship ($\beta = 1$). However, in highly polarized faradaic electrodes, redox processes become more dominant and give rise to drift dominant relocation processes. This scenario generally corresponds to a 1/f^2 relationship or $\beta = 2$.[29] Based on these postulates, we would expect more faradaic influence/drift when biasing in the sub-threshold regime at -4.2 V, whereas biasing in the saturation regime only places V_g at -1 V. If redox reactions from ions within the buffer solution are the primary cause of noise phenomena and faradaic interactions within the system, a change in β should be observed with varying ionic strength, which indeed is the case as shown in Fig. 3(b). More specifically, this determines the point at which the noise phenomenon shifts from a diffusion dominant process to a drift dominant one via the introduction of faradaic activities.

Based on the data from Figs. 2 and 3, we can make a few observations. The first is that an applied gate bias of -1 V appears to be insufficient to trigger electrochemical or faradaic reactions and can be considered as an IPE-style electrode dominated by diffusion processes

for the ionic strengths in this study. We do note that there are some deviations from "ideal" behavior, i.e., the β values for $10^{-2} \times$ and $10^{-5} \times$ reach upward of 1.23 and 1.21, respectively. However, given the erratic behavior of noise and probable minor influences of drift processes even in a diffusion dominant scenario, some level of deviation is expected. In the sub-threshold regime, the noise characteristics show 1/f behavior until $10^{-5} \times$ PBS. After this point, the noise is likely some combination of both drift and diffusion processes, resulting in a β value somewhere between 1 and 2. This observation mirrors studies from others who proposed a noise model with contributions from C_1/f and C_2/f^2 components where C_1 and C_2 are constants.[31] Once the $10^{-3} \times$ concentration is reached, drift can be considered the dominant process. It must follow that even with the -4.2 V bias on the gate electrode, at sufficiently low ionic strengths, there are negligible to minor faradaic processes, but this gradually changes as the prevalence of salt and ionic species is increased. Indeed, -4.2 V appears to be able to trigger some redox reactions at "medium" ionic strengths and becomes dominant at higher strengths, which are common in physiological media.

Considering the difference in the two biasing regimes for solutions with high ionic strengths, we then investigate how the β value varies with the gate bias. Figure 3(c) shows the β value as a function of gate bias for PBS $1 \times$ electrolyte. As expected, we observe a gradual increase from $\beta = 1$ to $\beta = 2$ as we increase the magnitude of the gate bias from relatively weak biasing to higher biases. The device exhibits 1/f noise characteristics (roughly static $\beta = 1$) until a gate bias slightly greater than -1 V. After this point, it continues to increase until it reaches $\beta = 2$ at -4.2 V. This increase in β over the region from approximately -1 V to -4.2 V is also consistent with previous observations of water dissociation at sufficient biases (<-1 V).[32–34] However, as discussed previously, at low ionic strengths ($\approx 10^{-6} \times$ PBS), the dominant process is still a diffusion process even under a high gate bias. This suggests that the low frequency noise due to redox electrochemical activities is impacted mainly by ionic reactions in solutions with high ionic strengths under a high bias and water dissociation is not a dominant factor. To validate this, we measured the low frequency noise in DI water under the biases of -4.2 V and -1 V. The β values

are 1.31 and 1.14, respectively, suggesting that the water spitting has indeed a relatively minor impact on the noise behavior. Furthermore, looking at SNR values in each biasing regime, we can make two observations: first, the device displays a higher SNR when operated in the sub-threshold regime for a given ionic strength. Second, the ionic strength has a significant impact on the SNR in both the sub-threshold and saturation regimes. The SNR values differ by roughly one order of magnitude across the ionic strengths used due to the measured change in current noise. Thus, we assert that the ionic strength can substantially influence the device SNR. It should be pointed out that though this work is based on the AlGaN/GaN HEMT platform, these observations should be applicable to FET-based biosensors on other material systems such as Si MOSFETs, carbon nanotube FETs, graphene, and 2D semiconductor FETs. The differences would likely be the noise amplitudes and the onset of ionic strengths that a faradic process becomes predominant. Therefore, careful consideration should be given when performing measurements in ionic solutions or physiological buffers on these FET-based biosensors.

In conclusion, we have shown how the noise characteristics for an AlGaN/GaN biosensor platform can influence real sensing applications to a greater or lesser degree depending on measurement conditions. The results show that gate voltage bias as well as the ionic strength of the aqueous solution used affects the maximum sensitivity (or LOD) of the AlGaN/GaN device and noise of the sensor system. Across the range of ionic strengths tested, a change in the SNR of approximately one order is observed in both saturation and sub-threshold regimes. In the saturation regime, the device SNR is inversely proportional to the ionic strength as a result of electrical screening. Additionally, the SNR for this device is higher in the sub-threshold regime when compared to the on-state. The device displays $1/f$ noise characteristics commonly observed in electronic devices under sufficiently low gate biases in a wide range of ionic strengths. When the device is under a gate bias exceeding -1 V concomitantly with the usage of solutions above $10^{-5} \times$ PBS, the noise behavior exhibits a combination of both $1/f$ and $1/f^2$ (drift and diffusion) characteristics due to the introduction of faradic effects. Once the ionic strength reaches $10^{-3} \times$ PBS, with a high gate bias (-4.2 V), the low frequency noise behaves predominantly as $1/f^2$, indicating a drift dominant process. While this work is done solely on the AlGaN/GaN HEMT platform, we believe that the findings found herein will apply and be relevant to other FET-based sensing platforms.

DATA AVAILABILITY

The data that support the findings of this study are available within this article.

REFERENCES

[1] N. Bhalla, M. D. Lorenzo, G. Pula, and P. Estrela, Biosens. Bioelectron. **54**, 109 (2014).
[2] B. M. Paddle, Biosens. Bioelectron. **11**, 1079 (1996).
[3] T. K. Sharma, R. Ramanathan, R. Rakwal, G. K. Agrawal, and V. Bansal, Proteomics **15**, 1680 (2015).
[4] R. Thapa, S. Alur, K. Kim, F. Tong et al., Appl. Phys. Lett. **100**, 232109 (2012).
[5] Y. Wang and W. Lu, Phys. Status Solidi A **208**, 1623 (2011).
[6] B. S. Kang, S. J. Pearton, J. J. Chen, J. W. J. F. Ren, R. J. Therrien, P. Rajagopal, J. C. Roberts, E. L. Piner, and K. J. Linthicum, Appl. Phys. Lett. **89**, 122102 (2006).
[7] S. Alur, R. Thapa, T. Ganaprakasa, Y. Wang, Y. Sharma, E. Javalosa, E. Smith, C. Ahyi, A. Simonian, M. Bozack, J. Williams, and M. Park, Phys. Status Solidi C **8**, 2483 (2011).
[8] J. Juan-Colás, A. Parkin, K. E. Dunn, M. G. Scullion, T. F. Krauss, and S. D. Johnson, Nat. Commun. **7**, 12769 (2016).
[9] M. J. Bañuls, R. Puchades, and A. Maquieira, Anal. Chim. Acta **777**, 1 (2013).
[10] J. Wang, Chem. Rev. **108**, 814 (2008).
[11] J. Wang, Electroanalysis **17**, 7–14 (2005).
[12] K. D. Vos, I. Bartolozzi, E. Schacht, P. Bienstman, and R. Baets, Opt. Express **15**, 7610 (2007).
[13] M. Lee and P. M. Fauchet, Opt. Express **15**, 4530 (2007).
[14] S. Chowdhury, M. Wong, B. Swenson, and U. Mishra, IEEE Electron Dev. Lett. **33**, 41 (2012).
[15] M. Kanechika, M. Sugimoto, N. Soejima, N. Ueda, O. Ishiguro, M. Kodama, E. Hayashi, K. Itoh, T. Uesugi, and T. Kachi, Jpn. J. Appl. Phys., Part 2 **46**, L503 (2007).
[16] G. Steinhoff, O. Purrucker, M. Tanaka, M. Stutzmann, and M. Eickhoff, Adv. Funct. Mater. **13**, 841 (2003).
[17] X. Wen, S. Wang, Y. Wang, L. Lee, and W. Lu, Chin. Sci. Bull. **58**, 2601 (2013).
[18] P. Casal, X. Wen, S. Gupta, T. Nicholson, Y. Wang, A. Theiss, B. Bhushan, L. Brillson, W. Lu, and S. Lee, Philos. Trans. R. Soc., A **370**, 2474 (2012).
[19] F. Mohd-Yasin, D. J. Nagel, and C. E. Korman, Meas. Sci. Technol. **21**, 012001 (2010).
[20] D. Landheer, G. Aers, W. R. McKinnon, M. J. Deen, and J. C. Ranuarez, J. Appl. Phys. **98**, 044701 (2005).
[21] M. J. Deen, M. W. Shinwari, J. C. Ranuarez, and D. Landheer, J. Appl. Phys. **100**, 074703 (2006).
[22] M. W. Shinwari, M. J. Deen, and D. Landheer, Microelectron. Reliab. **47**, 2025 (2007).
[23] N. K. Rajan, D. A. Routenberg, and M. A. Reed, Appl. Phys. Lett. **98**, 264107 (2011).
[24] G. Steinhoff, B. Baur, G. Wrobel, S. Ingebrandt, A. Offenhäusser et al., Appl. Phys. Lett. **86**, 033901 (2005).
[25] S. Chomean, T. Potipitak, C. Promptmas, and W. Ittarat, Clin. Chem. Lab. Med. **48**, 1247 (2010).
[26] X. P. Gao, G. Zheng, and C. M. Lieber, Nano. Lett. **10**, 547 (2010).
[27] I. Heller, J. Mannik, S. G. Lemay, and C. Dekker, Nano. Lett. **9**, 377 (2009).
[28] F. N. Hooge, Phys. Lett. **29**, 139 (1969).
[29] A. Hassibi, R. Navid, R. W. Dutton, and T. H. Lee, J. Appl. Phys. **96**, 1074 (2004).
[30] X. Jiang, S. Nesic, F. Huet, B. Kinsella, B. Brown, and D. Young, J. Electrochem. Soc. **159**, C283 (2012).
[31] M. P. Das and M. Bhuyan, Sens. Transducers **149**, 102 (2013).
[32] L. J. Chenga and H. C. Chang, Biomicrofluidics **5**, 046502 (2011).
[33] C. Bassignana and H. Reiss, Membr. Sci. **15**, 27 (1983).
[34] G. Grossman, J. Phys. Chem. **80**, 1616 (1976).